Systematic determination of absolute absorption cross-section of individual carbon nanotubes

Kaihui Liu[a,b,1], Xiaoping Hong[a,1], Sangkook Choi[a,c], Chenhao Jin[a], Rodrigo B. Capaz[a,d], Jihoon Kim[a], Wenlong Wang[e], Xuedong Bai[e], Steven G. Louie[a,c], Enge Wang[f], and Feng Wang[a,c,g,2]

[a]Department of Physics, University of California, Berkeley, CA 94720; [b]State Key Laboratory for Mesoscopic Physics, School of Physics, Peking University, Beijing 100871, China; [c]Materials Science Division, Lawrence Berkeley National Laboratory, Berkeley, CA 94720; [d]Instituto de Física, Universidade Federal do Rio de Janeiro, 21941-972, Rio de Janeiro, RJ, Brazil; [e]Institute of Physics, Chinese Academy of Sciences, Beijing 100190, China; [f]International Center for Quantum Materials and Collaborative Innovation Center of Quantum Matter, Peking University, Beijing 100871, China; and [g]Kavli Energy NanoSciences Institute at the University of California, Berkeley, and the Lawrence Berkeley National Laboratory, Berkeley, CA 94720

Edited by Paul L. McEuen, Cornell University, Ithaca, NY, and approved April 15, 2014 (received for review October 9, 2013)

Optical absorption is the most fundamental optical property characterizing light–matter interactions in materials and can be most readily compared with theoretical predictions. However, determination of optical absorption cross-section of individual nanostructures is experimentally challenging due to the small extinction signal using conventional transmission measurements. Recently, dramatic increase of optical contrast from individual carbon nanotubes has been successfully achieved with a polarization-based homodyne microscope, where the scattered light wave from the nanostructure interferes with the optimized reference signal (the reflected/transmitted light). Here we demonstrate high-sensitivity absorption spectroscopy for individual single-walled carbon nanotubes by combining the polarization-based homodyne technique with broadband supercontinuum excitation in transmission configuration. To our knowledge, this is the first time that high-throughput and quantitative determination of nanotube absorption cross-section over broad spectral range at the single-tube level was performed for more than 50 individual chirality-defined single-walled nanotubes. Our data reveal chirality-dependent behaviors of exciton resonances in carbon nanotubes, where the exciton oscillator strength exhibits a universal scaling law with the nanotube diameter and the transition order. The exciton linewidth (characterizing the exciton lifetime) varies strongly in different nanotubes, and on average it increases linearly with the transition energy. In addition, we establish an empirical formula by extrapolating our data to predict the absorption cross-section spectrum for any given nanotube. The quantitative information of absorption cross-section in a broad spectral range and all nanotube species not only provides new insight into the unique photophysics in one-dimensional carbon nanotubes, but also enables absolute determination of optical quantum efficiencies in important photoluminescence and photovoltaic processes.

polarization microscope | homodyne detection | carbon nanotube optical spectroscopy | excitons in carbon nanotubes

Single-walled carbon nanotubes (SWNTs), a model one-dimensional nanomaterial system, constitute a rich family of structures (1). Each single-walled nanotube structure, uniquely defined by the chiral index (n,m), exhibits distinct electrical and optical properties (2–5). Quantitative information of SWNT absorption cross-section is highly desirable for understanding nanotube electronic structures, for evaluating quantum efficiency of nanotube photoluminescence (5, 6) and photocurrent (7–9), and for investigating the unique many-body effects in 1D systems (10–16). Despite its obvious importance, reliable experimental determination of nanotube absorption cross-section at the single-tube level is still challenging (17). Previous absorption measurements on ensemble nanotube samples only provide averaged behavior (18–20). Recent absorption studies of individual nanotubes, suffering from small absorption signals and/or slow laser-frequency scanning, cannot determine the absolute absorption cross-section and are limited in achievable spectral range (15, 21–23).

We demonstrate here a high-sensitivity polarization-based homodyne method to measure nanotube absorption spectra. By manipulating the light polarization, we enhanced the nanotube-induced transmission contrast, $\Delta I/I$, by two orders of magnitude, and this enhanced transmission contrast can be quantitatively related to nanotube absorption cross-section along and perpendicular to the nanotube axis. Using this polarization control together with supercontinuum laser source, we realized high-throughput and broadband absorption measurements at the single-tube level; combined with electron diffraction technique on the same tube, it enables absolute determination of absorption cross-sections of individual chirality-defined nanotubes, to our knowledge for the first time. We obtained quantitative absorption spectra of over 50 SWNTs of different chiralities, and established a phenomenological formula for absorption cross-sections of different nanotubes. The chirality-dependent nanotube absorption spectra reveal unique 1D photophysics in nanotubes, including a universal scaling behavior of exciton oscillator strength and of exciton resonance linewidth.

Results

Experimental Design. In 2D monolayer graphene, a universal absorption of ~2.3% in the visible and near infrared range was predicted and observed (24, 25). For 1D nanotube with light

Significance

Determination of optical absorption cross-section is of central importance to understanding a material; however, its realization on individual nanostructures, such as carbon nanotubes, is experimentally challenging due to the small extinction signal using conventional transmission measurements. Here we develop a technique based on polarization manipulation to enhance the sensitivity of single-nanotube absorption spectroscopy by two orders of magnitude. We systematically determine absorption cross-section over broad spectral range at the single-tube level for more than 50 chirality-defined single-walled nanotubes. Our data reveals chirality-dependent one-dimensional photophysics through the behaviors of exciton oscillator strength and lifetime. We also establish an empirical formula to predict absorption spectrum of any nanotube, which provides the foundation to determine quantum efficiencies in important photoluminescence and photovoltaic processes.

Author contributions: K.L., X.H., and F.W. designed research; K.L. and X.H. performed research; K.L., X.H., S.C., C.J., R.B.C., S.G.L., E.W., and F.W. analyzed data; K.L., X.H., S.C., C.J., R.B.C., J.K., W.W., X.B., S.G.L., E.W., F.W. wrote the paper; K.L., J.K., and W.W. grew the sample; and K.L. and X.B. managed TEM characterization.

The authors declare no conflict of interest.

This article is a PNAS Direct Submission.

[1]K.L. and X.H. contributed equally to this work.

[2]To whom correspondence should be addressed. E-mail: fengwang76@berkeley.edu.

This article contains supporting information online at www.pnas.org/lookup/suppl/doi:10.1073/pnas.1318851111/-/DCSupplemental.

polarized along its axis, the typical absorption of a single nanotube is 2–3 orders of magnitude smaller, i.e., at 10^{-4} to 10^{-5}, due to its nanometer diameter compared with micrometer illumination beam size. This small signal is easily overwhelmed by intensity fluctuation of the light source, making it difficult to measure single-tube absorption with conventional transmission spectroscopy. However, realizing that conventional transmission measurement is just one form of homodyne detection, we can measure the nanotube absorption cross-section with high sensitivity by optimizing the homodyne process.

From the interferometric point of view, our technique is a special example of homodyne detection. This method has been recently extended to carbon nanotubes with manipulation of polarizations (26, 27). In a homodyne measurement, the detected light intensity change ($\Delta I/I$) originates from the interference between the signal (E_s) and local oscillator electric field (E_{LO}). Therefore,

$$\frac{\Delta I}{I}=\frac{|E_{LO}+E_s|^2-|E_{LO}|^2}{|E_{LO}|^2}$$
$$=\frac{2|E_s|}{|E_{LO}|}\cos\phi \xrightarrow{\text{Transmission}} \frac{\Delta T}{T}=\frac{2|E_{NT}|}{|E_{in}|}\cos\phi=-\alpha, \qquad [1]$$

where ϕ is the relative phase between Es and E_{LO}, and we have ignored the small $|E_s|^2$ term. The equation on the right describes conventional nanotube transmission measurements, where E_s and E_{LO} are, respectively, the nanotube forward-scattering wave (E_{NT}) and the unperturbed incident light (E_{in}), and α is the nanotube absorption. If we can control E_s and E_{LO} with precisely defined relations to E_{NT} and E_{in}, we can potentially greatly enhance optical detection contrast $\Delta I/I$, and from it determine the absolute nanotube absorption cross-section; this can be achieved through polarization manipulation as shown in Fig. 1*A*. Two nearly crossed polarizers (with a small deviation angle δ) were used to control the incident and outgoing light polarization, and two polarization-maintaining objectives were placed confocally between this polarizer pair. Suspended individual nanotubes were positioned at the focus of the objectives and with an angle of 45° with respect to the first polarizer. This configuration varies both local oscillator E_{LO} and signal E_s in a precise matter, where local oscillator is greatly reduced by $E_{LO}=E_{in}\sin\delta$, and the signal is related to the initial nanotube field by $E_s\approx(E_{NT}^{//}-E_{NT}^{\perp})/\sqrt{2}$, where $E_{NT}^{//}$ and $E_{NT}^{\perp}$ are nanotube field along and perpendicular to the nanotube axis, respectively. With this polarization control, we can obtain the polarization-dependent nanotube absorption through the enhanced homodyne optical contrast directly using (*SI Text, Determine the Nanotube Absorption Constants $\alpha_{//}$ and $\alpha_{\perp}$ from the Homodyne Modulation Signal*)

$$-\frac{\Delta I}{I}(\delta)=\frac{\alpha_{//}-\alpha_{\perp}}{2}\mathrm{ctg}(\delta)+\frac{\alpha_{//}+\alpha_{\perp}}{2}, \qquad [2]$$

where $\alpha_{//}$ and $\alpha_{\perp}$ are nanotube absorption constants for light polarized parallel and perpendicular to the nanotube axis, respectively. Here, $(\alpha_{//}-\alpha_{\perp})/2$ characterizes the strong depolarization effect of nanotubes; it gives rise to a greatly enhanced optical contrast $\Delta I/I$ at small δ, which can reach ~1% (compared with 10^{-4} in conventional transmission change) and becomes easily detectable.

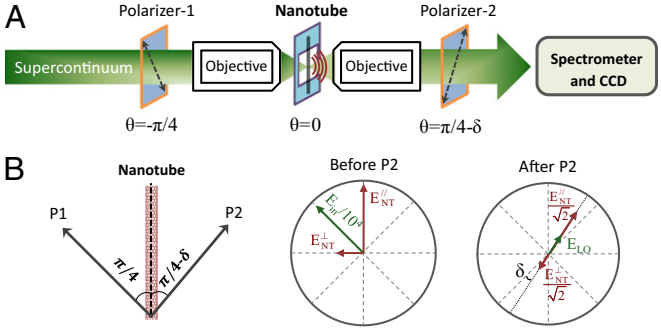

Fig. 1. Scheme of polarization-optimized homodyne detection for single-nanotube absorption. (*A*) Two nearly crossed polarizers (with a small deviation angle δ) were used to control the incident and outgoing light polarization, and two polarization-maintaining objectives were placed confocally between this polarizer pair. Suspended individual nanotubes were positioned at the focus of the objectives and with an angle of $\pi/4$ with respect to the first polarizer polarization. We used broadband supercontinuum laser (spectral range 450–850 nm) as the light source and a spectrometer equipped with a silicon linear array for fast wide-spectral detection. (*B*) Interference between E_{in} and E_{NT} after the nanotube gives rise to nanotube extinction, whereas interference between $E_s(\approx(E_{NT}^{//}-E_{NT}^{\perp})/\sqrt{2})$ and E_{LO} ($=E_{in}\sin\delta$) after polarizer 2 generates the final homodyne signal. Given that E_{LO}: $E_{in}\sim10^{-2}$ and E_s: $E_{NT}\sim1/\sqrt{2}$ with suitable polarizer setting, the enhanced homodyne modulation signal $\Delta I/I$ can be two orders of magnitude higher than the transmission change $\Delta T/T=-\alpha$; it enables high sensitivity measurements of nanotube absorption α. The δ angle is exaggerated for better visualization.

Determination of Absolute Absorption Cross-Section. The power of our technique is demonstrated in Fig. 2, which displays $\Delta I/I$ spectra from a SWNT using different polarization settings. The chiral index of this nanotube was independently determined as (24,24) from its electron diffraction pattern (Fig. 2*A* and Fig. S1) (28). By gradually decreasing δ (the deviation angle from the crossed polarizer position as labeled in Fig. 1*A* and Fig. S2) from 5° to 0.5°, the resulting modulation signal $|\Delta I/I|$ increases steadily to 1% level at peak positions (Fig. 2*B*). Fig. 2*C* further shows that when δ crosses zero, the local oscillator E_{LO} changes sign, as does the homodyne interference modulation $\Delta I/I$. This new polarization scheme, coupled with supercontinuum illumination and array detections, enables us to obtain single-nanotube $\Delta I/I$ spectra across a wide spectral range in a few seconds, orders of magnitude faster than previous approaches (15, 21–23).

The spectra of $\Delta I/I$ as a function of δ allow direct determination of both $\alpha_{//}$ and $\alpha_{\perp}$. Fig. S3 displays $\alpha_{//}$ and $\alpha_{\perp}$ over a broad spectral range for the (24,24) SWNT, which have values in the order of 10^{-4} as expected. Nanotube absorption cross-sections are proportional to $\alpha_{//}$ and $\alpha_{\perp}$, and their absolute values can be obtained once the illumination beam size is known. We determine the focused supercontinuum beam profile at high accuracy by systematically measuring the absorption spectra with nanotubes at different positions in the focused beam (*SI Text, Determine the Absolute Absorption Cross-Section from Absorption Constants*). With this information, we obtained spectra of optical absorption cross-sections per atom along both parallel ($\sigma_{//}$) and perpendicular ($\sigma_{\perp}$) polarizations for the (24,24) SWNT, which is displayed in Fig. 2*D*. We performed such absorption measurements on 57 chirality identified SWNTs, and it allows us to systematically examine polarization-dependent absorption cross-section in different nanotube species, to our knowledge for the first time. The $\sigma_{//}$ spectra show prominent and different exciton transition peaks in different nanotubes. These chirality-dependent exciton transitions provide rich information on chirality-dependent nanotube photophysics, as we describe later. The $\sigma_{\perp}$ spectra, however, show a small and finite perpendicular absorption (~1/4 of the average $\sigma_{//}$ value), and they are largely featureless.

We first examine briefly the $\sigma_{\perp}$ spectra, which have never been probed at the single nanotube level before. The small magnitude of $\sigma_{\perp}$ can be attributed to depolarization effects (18, 19, 29, 30), but its lack of any resonance features is surprising at the first look. It is widely known that perpendicularly polarized light can excite transitions between adjacent cutting lines due to angular momentum selection rule (1). One naturally expects resonance

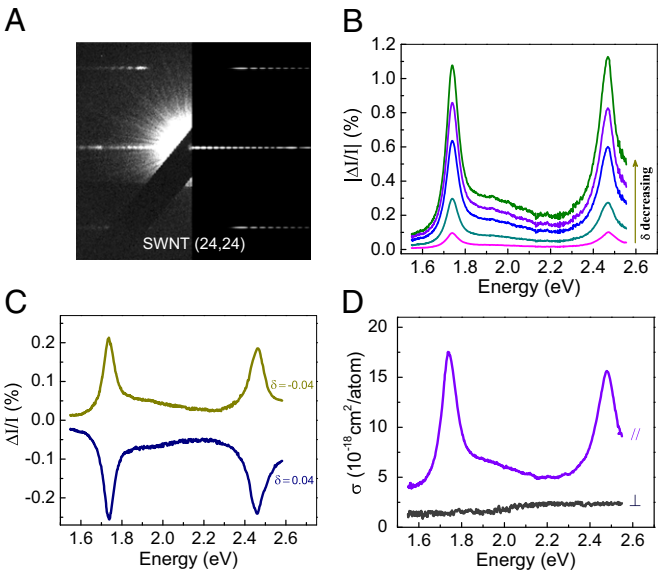

Fig. 2. Representative data for polarization-optimized homodyne detection of single-nanotube absorption. (*A*) Electron diffraction patterns (*Left*: experimental; *Right*: simulated) uniquely determine the chiral index of this nanotube as (24,24). The black diagonal feature in the experimental pattern is from the blocking stick inside the TEM for dark-field imaging. (*B*) Homodyne modulation signal ($|\Delta I/I|$) at various values of δ as in Fig. 1*A*. With δ decreasing from 5 to 0.5°, the signal at resonances gradually increases to the 1% level. (*C*) Modulation signal at $\delta = \pm 0.04$; it shows interference signature that when δ crosses zero, local oscillator E_{LO} changes sign and so does the homodyne interference modulation $\Delta I/I$. (*D*) The absolute absorption cross-section per carbon atom with both parallel (*//*) and perpendicular (⊥) light polarization to nanotube axis. The $\sigma_{//}$ spectrum shows clear resonance peaks corresponding to the exciton transitions, whereas $\sigma_{\perp}$ is mostly featureless. For all studied SWNTs, $\sigma_{\perp}$ has an integrated absorption between one-fifth and one-third of that in $\sigma_{//}$ due to depolarization effect in 1D nanotubes.

features associated with these exciton transitions in $\sigma_{\perp}$ spectra. Indeed, prominent absorption peak corresponding to S_{12} and S_{21} transitions have been observed in semiconducting nanotubes with perpendicular polarization excitation (6). However, here we do not observe any resonances in our $\sigma_{\perp}$ spectra, where transitions between higher subbands are probed. Detailed theoretical analysis shows that although transitions between adjacent cutting lines are symmetry allowed, their matrix elements are always zero close to the band gap because they fail to conserve pseudospin, except for the S_{12} and S_{21} transitions (31) (*SI Text, Cutting Line Scheme of Optical Transitions with Angular Momentum Difference of ±ħ in Carbon Nanotubes*). This matrix element effect strongly suppresses exciton transition (as well as van Hove singularity at the band edge), resulting in no spectral resonances for higher-order transitions under perpendicularly polarized light (Fig. S4). Away from the band edge, the transition matrix element becomes finite and results in the finite but largely featureless $\sigma_{\perp}$, as we observe experimentally.

Systematic Analysis of Absorption Cross-Section. Below, we focus on $\sigma_{//}$ spectra in chirality-defined SWNTs. Fig. 3 displays four representative parallel polarization spectra (black lines) in semiconducting [(18,14) and (25,23)] and metallic [(16,16) and (24,24)] nanotubes, where the chiral indices were independently determined by the electron diffraction techniques. All $\sigma_{//}$ spectra in Fig. 3 are characterized by sharp optical resonances arising from excitonic transitions (10–16) and a broad continuum background; they provide a wealth of information on the unique nanotube photophysics.

Discussion

Approximation Sum Rule. We first note that for all nanotubes, the average absorption cross-section is $\sim 7.6 \times 10^{-18}$ cm^2 per atom, which corresponds to an integrated cross-section (Σ_A) of 7.1×10^{-18} eV·cm^2 per atom between the spectral range 1.55–2.48 eV, the same as Σ_A of graphene in the same range (24, 25). Fig. 4*A* shows in detail the distribution of Σ_A in different nanotubes (dots), which converges on the graphene value (dashed line). The physical origin for this convergence is an approximated f-sum rule, where the integrated oscillator strength per atom over a sufficiently large spectral range should be the same for all graphitic structures. The agreement between nanotubes and graphene values provides an independent confirmation of the accuracy of our nanotube absorption cross-section results. (The slight variation in nanotube values is presumably due to the different distribution of resonant peaks in different nanotubes and the finite integrated energy range.)

Chirality and Transition-Dependent Exciton Oscillator Strength. To quantitatively describe the chirality-dependent absorption features in different nanotubes, we introduce a phenomenological model composed of a discrete exciton peak and corresponding continuum absorption for each subband. The exciton transitions are Lorentzian resonances, each characterized by its resonance energy E_p, resonance width Γ_p, and oscillator strength (integrated cross-section) Σ_p. Here, p is an integer indexing optical transitions of both semiconducting (S_{ii}) and metallic nanotubes (M_{ii}) starting from 1 in the order of S_{11}, S_{22}, M_{11}, S_{33}, S_{44}, M_{22}, S_{55}, S_{66}, M_{33}, S_{77},... (16). The "continuum" absorption, including the contribution from band-to-band transitions as well as phonon sidebands and higher-order exciton transitions, is approximated empirically by a Lorentzian broadened form of the function $\Theta[E-(E_p+\Delta_p)]\times(1/\sqrt{E-(E_p+\Delta_p)})$. Here, Θ is the

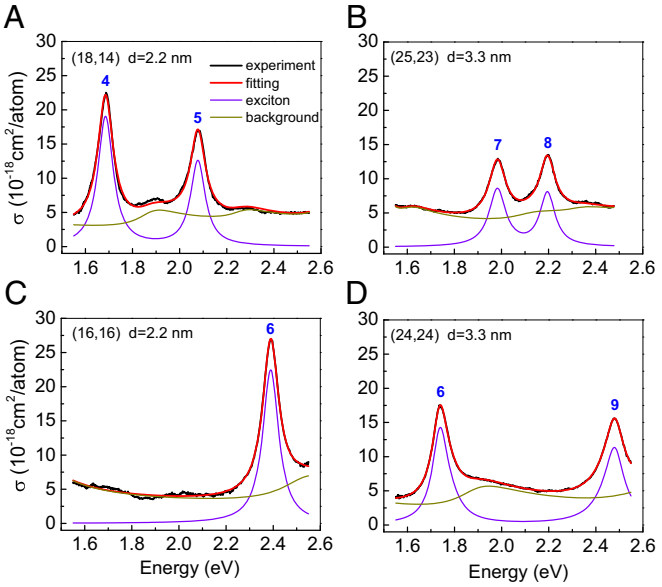

Fig. 3. Representative absorption cross-section spectra of four nanotubes. (*A*) Semiconducting (18,14). (*B*) Semiconducting (25,23). (*C*) Metallic (16,16). (*D*) Metallic (24,24). Black, red, violet, and dark yellow lines are experimental data, phenomenological fitted total absorption, exciton component, and continuum component, respectively. The integer number *p* at each peak indexes the optical transition type as described in the text. The resonant peaks show symmetric shape and reveal the exciton nature of nanotube optical transitions, while an obvious continuum background exists. The phenomenological model described in the text reproduces the absorption spectra nicely. The exciton transition energy, oscillator strengths, and line width vary significantly with the nanotube species and transition index *p*.

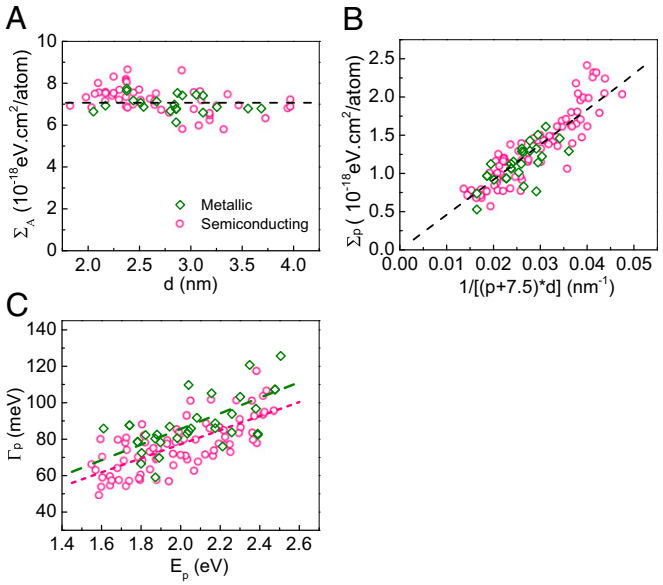

Fig. 4. Tube-dependent exciton oscillator strength and transition linewidth in 57 SWNTs. The diamonds and the circles represent data from 18 metallic and 39 semiconducting nanotubes, respectively. (*A*) Integrated absorption cross-section in the energy range of 1.55 to 2.48 eV. All of the data converge to the value of graphene integrated over the same energy region (dashed line). This convergence originates from an approximated f-sum rule. (*B*) Tube-dependent exciton oscillator strength is described by a universal scaling law of $4.6\times10^{-24}/[(p+7.5)\cdot d]$ eV·cm^3 per atom (dashed line), where d is nanotube diameter and p is transition order indexing both semiconducting and metallic nanotube optical transitions. Metallic and semiconducting nanotubes, surprisingly, exhibit similar exciton oscillator strength, although they are characterized by significantly different electron-hole interactions. (*C*) Exciton transition linewidth in different nanotubes. On average, the linewidth increases linearly with the transition energies. The higher slope for metallic nanotube (long-dashed line) than that for semiconducting nanotube (short-dashed line) reveals (on average) slightly shorter exciton lifetime due to coupling to free electrons in metallic nanotubes. The large scattering present in the exciton linewidth suggests that ultrafast dynamics of the excited states can vary dramatically with the exact nanotube electronic structure.

heavyside step function, Δ_p is the offset of continuum edge relative to the exciton transition, and the second term models the 1D density of states close to the band edge [*SI Text, Empirical Formula for Absorption Cross-Section of an (n,m) Nanotube*]. Red lines in Fig. 3 show that our phenomenological model nicely reproduces the experimental absorption spectra, with violet and dark yellow lines showing the exciton and continuum contribution, respectively. We note that the continuum absorption constitutes a significant portion of the total nanotube absorption oscillator strength, which has never been appreciated previously. The relative importance of continuum absorption increases with the nanotube diameter and the transition index p.

Exciton resonances, the most prominent features in the absorption spectra, encode rich 1D nanotube physics in their chirality-dependent behavior: (*i*) The exciton absorption oscillator strength provides new information on electron-hole interaction strength in the 1D nanotubes; (*ii*) the exciton transition linewidth, arising from the finite exciton lifetime, reveals the ultrafast relaxation dynamics of excited states; and (*iii*) the exciton transition energies and their dependence on nanotube species observed in absorption spectra here provide a valuable confirmation of the recent assignment established using Rayleigh scattering spectroscopy (16) with an accuracy of 10 meV.

The exciton takes its oscillator strength from band-to-band transitions due to the electron-hole correlation (12–15); its value depends on both the interband optical transition matrix element and the exciton wave function at zero electron-hole separation. We observe in the experimental spectra (Fig. 3) that the exciton oscillator strength decreases significantly in large diameter nanotubes. A systematic examination reveals that the tube-dependent exciton oscillator strength can be described by a universal scaling law, $\Sigma_p \sim 1/(p+7.5)d$, as displayed in Fig. 4*B*. For semiconducting nanotubes, this scaling law can be understood theoretically using a model description of the excitonic effects, and the magnitude of observed exciton oscillator strengths agrees well with our theoretical predictions (32).

Fig. 4*B* also shows that the exciton oscillator strengths in metallic (diamonds) and semiconducting (circles) nanotubes have similar magnitude and fall on the same curve. This behavior appears surprising, because the electron-hole interactions are expected to be much weaker in metallic nanotubes due to free electron screening. Naively, the resulting exciton transition should have significantly smaller oscillator strength. Previous ab initio calculations (12, 13), however, showed that the oscillator strength from excitons in metallic nanotubes are comparable to those in semiconducting tube, although no systematic analysis was carried out. Further effort will be required to understand quantitatively the experimental data here, and it could lead to deeper insight into many-body interactions in 1D nanotubes.

Transition Energy-Dependent Exciton Linewidth. The optical linewidth of exciton transitions (for $P > 1$) originates mainly from exciton lifetime broadening due to electron–electron and electron–phonon interactions. Ultrafast evolution of the exciton states plays a key role in important optoelectronic processes such as multiexciton generation (9) and impact ionization (2). Our data provide a unique opportunity to investigate the chirality-dependent ultrafast dynamics in SWNTs. We plot in Fig. 4*C* the observed exciton linewidth in semiconducting (circles) and metallic (diamonds) nanotubes as a function of exciton transition energies; it shows that (*i*) the exciton linewidth, on average, increases linearly with transition energy and (*ii*) there is a large variation of exciton lifetime in different nanotube species.

The linear increase of average linewidth indicates a shorter exciton lifetime scales inversely with transition energy. This faster relaxation can be approximately attributed to increased phase space for electron–electron and electron–phonon scatterings at higher energy. Similar increases in excited-state relaxation rate with energy have been observed in studies of graphite (33) and low-order transitions in carbon nanotubes (34). The large variation of exciton lifetime, even for transitions at the same energy, indicates that the ultrafast electron relaxation may depend sensitively on the exact electronic structure, an important effect that to our knowledge has been previously unexplored; we hope our experimental data can stimulate their theoretical study to gain more insight on ultrafast electron dynamics in 1D systems.

Empirical Description of (n,m) Nanotube Absorption Cross-Section. Last, we are able to develop an empirical formula for optical absorption spectra in all nanotubes (with diameter ranging from 1.2 to 3.2 nm) using the established relations for exciton oscillator strength and resonance width described above (Table S1). This phenomenological description reproduces the absorption spectra within 20% accuracy in our experimental energy region 1.45–2.55 eV [see the detailed description and example (Fig. S5) in *SI Text, Empirical Formula for Absorption Cross-Section of an (n,m) Nanotube*]. Such empirical formula of optical absorption cross-section for a wide variety of nanotubes across the visible spectral range will be a valuable reference for determining quantum efficiency of important optical processes such as photoluminescence and photovoltaics.

Methods

Sample Preparation and Chiral Index (n,m) Characterization. In this study we combined single-tube absorption spectroscopy and electron-diffraction techniques on the same individual suspended nanotubes (*SI Text, Determine the Chiral Index and Absorption Spectrum of the Same Individual Carbon Nanotube*). The experimental scheme is illustrated in Fig. S1. Suspended long nanotubes were grown by chemical vapor deposition (CVD) across open-slit structures (~30 × 500 μm) fabricated on silicon substrates. We used methane in hydrogen (CH_4:H_2 = 1:2) as gas feedstock and a thin film (~0.2 nm) of Fe as the catalyst for CVD growth at 900 °C (35). This growth condition yields extremely clean isolated nanotubes free of amorphous carbon and other adsorbates. We determined the atomic structure of every nanotube from the electron diffraction pattern using nanofocused 80-keV electron beams in a JEOL 2100 transmission electron microscope (TEM) (28). By using the slit edges as spatial markers, the same individual nanotubes can be identified in both TEM and optical microscope setup.

Optical Measurement. Fig. 1*A* shows the scheme of the optical setup in our experiment; it includes a supercontinuum laser (Fianium SC-450), two Glan–Thomspon polarizers (Thorlabs GTH10), two Mitutoyo Objectives (Plan APO 50×, N.A. 0.42; we used effective N.A. 0.3 in the experiment), an optical grating (300 lines per millimeter; Thorlabs GTI50-03), a consumer camera (Nikon 5100) for imaging, and a 1D CCD array (Imaging Solution Group LW-ELIS-1024a-1394) for obtaining the spectrum.

The supercontinuum laser (470 ~ 850 nm) was used as our light source. The front objective serves to focus the supercontinuum light to the sample, and the second objective collects the nanotube scattering and transmission light. Polarizer 1 is placed in the incident beam with its transmission axis set 45° to the horizontal. Polarizer 2 is placed in the detection beam, and its polarization is controlled to be at a small angle δ to the vertical direction of polarizer 1.

We obtained the homodyne modulation spectrum by taking two sets of spectra with the nanotube in (I_i) and out (I_o) of the supercontinuum focus. The integration time of each spectrum was 5 ms. The modulation signal was obtained as $\Delta I/I = (I_i - I_o)/I_o$. By shifting the nanotube in and out of the focus quickly, we can take a high-quality modulation spectrum within 2 s.

Error Analysis. In our study, we determined the absolute absorption cross-section of SWNTs for electrical field polarized along the nanotube direction using Eqs. **S3** and **S5**, where

$$\alpha_{//} = \frac{\Delta I/I(-\delta) - \Delta I/I(\delta)}{2}\tan(\delta) - \frac{\Delta I/I(\delta) + \Delta I/I(-\delta)}{2},$$

and

$$\alpha_{//} = \sigma_{//}\frac{\sqrt{2\pi}}{S_0}\cdot\frac{d}{R}\cdot\exp\left(-\frac{2(x-x_c)^2}{R^2}\right).$$

The final absorption cross-section $\sigma_{//}$ is obtained by fitting a curve of absorption constant $\alpha_{//}$ vs. nanotube position x based on the above equations, where the laser beam center x_c and diameter R are also fitting parameters. S_0 is the area per carbon atom in graphitic lattice, and d is the nanotube diameter, which are discrete and exact values defined by the nanotube chiral index. The experiment uncertainty mainly arises from measurements of laser intensity change ΔI, polarizer angle δ, nanotube position x, and from systematic uncertainties of the technique, which we analyze in detail below.

Random Error from Measurements. ***Measurement uncertainty of I and ΔI.*** The measurement uncertainty of I and ΔI is affected by laser fluctuation, detector noise, and photon shot noises. The resulting uncertainty in $\alpha_{//}$ can be obtained from statistical fluctuations in multiple measurements. In our studies, we integrated 300 spectra, which leads to a fluctuation of $\alpha_{//}$ value within 2% at the absorption peak and ~6% for the nonresonant absorption. Fig. S3 shows a representative spectrum of $\alpha_{//}$, where the high quality of the spectra confirms that laser fluctuation-induced uncertainty is within our estimated range.

Determination of δ. We determine the polarization angle based on transmitted light intensity I_t after the second polarizer, which follows the equation $I_t = I_{in}\sin^2(\delta)$. In our experiment, we set δ at 0.04, which corresponds to a transmission of 1.6×10^{-3}. The uncertainty of δ arises from laser fluctuation and nonideal polarization extinction. The fluctuation of average laser intensity is less than 0.5%. The extinction ratio in our polarization microscope setup is 4×10^{-6}. Compared with the experimental transmission of 1.6×10^{-3}, the nonideal polarization leads to an uncertainty of 0.2% in δ. Overall, the measurements of δ adds an uncertainty of 0.5% in the value of $\alpha_{//}$.

Uncertainty of $\sigma_{//}$ from curve fitting of $\alpha_{//} = \sigma_{//}\sqrt{2\pi}/S_0\cdot\frac{d}{R}\cdot\exp(-2(x-x_c)^2/R^2)$. The uncertainties of $\alpha_{//}$ and position measurements contribute to the final uncertainty of through the curve fitting. Fig. S6 shows two representative fitting curves. From the fitting we estimate the uncertainty of $\sigma_{//}$ to be below 2–6%. The uncertainty of $\sigma_{//}$ shows a frequency dependence, and it is usually ~2% at an absorption resonance and ~6% for nonresonant absorption. This uncertainty in $\sigma_{//}$ is consistent with the fluctuation observed in the absorption cross-section spectra in Fig. 3.

Systematic Error. ***Plane-wave assumption.*** In our measurements we used focused light with an effective N.A. of 0.3, which does not have perfect in-plane linear polarization at the nanotube. The averaged in-plane field for N.A. = 0.3 is ~2% smaller than an ideal plane wave; it leads to a systematic overestimation of nanotube absorption cross-section by 2% in our measurements.

Error from neglecting higher-order terms. In Eq. **1**, we have neglected the higher-order term associated with $|E_{NT}|^2/|E_{LO}|^2$; this yields an uncertainty $\Delta\sigma/\sigma = \Delta\alpha/\alpha \sim E_{NT}/2E_{LO} < 1\%$.

Based on the above analysis, our determination of nanotube absorption cross-section has an uncertainty of ~4% at absorption resonances and an uncertainty of ~8% for background absorption.

An independent check of our measurement uncertainty is the comparison of nanotube absorption with that of graphene, as shown in Fig. 4*A*; it has a SD of 8%. This comparison sets an upper limit of our measurement uncertainty at 8%, which is consistent with the uncertainty estimated above.

ACKNOWLEDGMENTS. This study was supported by National Science Foundation (NSF) CAREER Grant 0846648; NSF Center for Integrated Nanomechanical Systems Grant EEC-0832819; NSF Grant DMR10-1006184; Department of Energy (DOE) Contract DE-AC02-05CH11231; DOE Molecular Foundry DE-AC02-05CH11231; Program 973 Project Grants 2012CB933003, 2013CB932601, and 2013CB932603; National Natural Science Foundation of China Grants 11027402, 91021007, 10974238, and 20973195; Chinese Academy of Sciences Grant KJCX2-YW-W35; Brazilian funding agencies Conselho Nacional de Desenvolvimento Científico e Tecnológico, Fundação de Amparo à Pesquisa do Estado do Rio de Janeiro, and Instituto Nacional de Ciência e Tecnologia Nanomateriais de Carbono (R.B.C.); and the National Program for Thousand Young Talents of China (K.L.). Computational resources have been provided by NSF through TeraGrid resources at National Institute for Computational Sciences and DOE at Lawrence Berkeley National Laboratory's National Energy Research Scientific Computing Center facility.

1. Dresselhaus MS, Dresselhaus G, Avouris P (2001) *Carbon Nanotubes: Synthesis, Structure, Properties, and Applications* (Springer, Berlin).
2. Chen J, et al. (2005) Bright infrared emission from electrically induced excitons in carbon nanotubes. *Science* 310(5751):1171–1174.
3. Sfeir MY, et al. (2006) Optical spectroscopy of individual single-walled carbon nanotubes of defined chiral structure. *Science* 312(5773):554–556.
4. Hertel T (2010) Carbon nanotubes: A brighter future. *Nat Photonics* 4(2):77–78.
5. Bachilo SM, et al. (2002) Structure-assigned optical spectra of single-walled carbon nanotubes. *Science* 298(5602):2361–2366.
6. Lefebvre J, Finnie P (2007) Polarized photoluminescence excitation spectroscopy of single-walled carbon nanotubes. *Phys Rev Lett* 98(16):167406.
7. Freitag M, et al. (2003) Photoconductivity of single carbon nanotubes. *Nano Lett* 3(8): 1067–1071.
8. Aguirre CM, et al. (2006) Carbon nanotube sheets as electrodes in organic light-emitting diodes. *Appl Phys Lett* 88(18):183104.
9. Gabor NM, Zhong Z, Bosnick K, Park J, McEuen PL (2009) Extremely efficient multiple electron-hole pair generation in carbon nanotube photodiodes. *Science* 325(5946): 1367–1371.
10. Ando T (1997) Excitons in carbon nanotubes. *J Phys Soc Jpn* 66(4):1066–1073.
11. Kane CL, Mele EJ (2004) Electron interactions and scaling relations for optical excitations in carbon nanotubes. *Phys Rev Lett* 93(19):197402.
12. Spataru CD, Ismail-Beigi S, Benedict LX, Louie SG (2004) Excitonic effects and optical spectra of single-walled carbon nanotubes. *Phys Rev Lett* 92(7):077402.
13. Malic E, Maultzsch J, Reich S, Knorr A (2010) Excitonic absorption spectra of metallic single-walled carbon nanotubes. *Phys Rev B* 82(3):035433.
14. Perebeinos V, Tersoff J, Avouris P (2004) Scaling of excitons in carbon nanotubes. *Phys Rev Lett* 92(25 Pt 1):257402.
15. Wang F, et al. (2007) Observation of excitons in one-dimensional metallic single-walled carbon nanotubes. *Phys Rev Lett* 99(22):227401.
16. Liu K, et al. (2012) An atlas of carbon nanotube optical transitions. *Nat Nanotechnol* 7(5):325–329.
17. Bohren CF, Huffman DR (1998) *Absorption and Scattering of Light by Small Particles* (Wiley-VCH, New York).
18. Islam MF, Milkie DE, Kane CL, Yodh AG, Kikkawa JM (2004) Direct measurement of the polarized optical absorption cross section of single-wall carbon nanotubes. *Phys Rev Lett* 93(3):037404.
19. Murakami Y, Einarsson E, Edamura T, Maruyama S (2005) Polarization dependence of the optical absorption of single-walled carbon nanotubes. *Phys Rev Lett* 94(8):087402.

20. Vialla F, et al. (2013) Chirality dependence of the absorption cross section of carbon nanotubes. *Phys Rev Lett* 111(13):137402.
21. Berciaud S, Cognet L, Poulin P, Weisman RB, Lounis B (2007) Absorption spectroscopy of individual single-walled carbon nanotubes. *Nano Lett* 7(5):1203–1207.
22. Herman LH, et al. (2012) Depolarization effect in optical absorption measurements of one- and two-dimensional nanostructures. *Appl Phys Lett* 101(12):123102.
23. Blancon J-C, et al. (2013) Direct measurement of the absolute absorption spectrum of individual semiconducting single-wall carbon nanotubes. *Nat Commun* 4:2542.
24. Nair RR, et al. (2008) Fine structure constant defines visual transparency of graphene. *Science* 320(5881):1308.
25. Mak KF, Shan J, Heinz TF (2011) Seeing many-body effects in single- and few-layer graphene: Observation of two-dimensional saddle-point excitons. *Phys Rev Lett* 106(4):046401.
26. Lefebvre J, Finnie P (2011) Polarized light microscopy and spectroscopy of individual single-walled carbon nanotubes. *Nano Res* 4(8):788–794.
27. Liu K, et al. (2013) High-throughput optical imaging and spectroscopy of individual carbon nanotubes in devices. *Nat Nanotechnol* 8(12):917–922.
28. Liu KH, et al. (2009) Direct determination of atomic structure of large-indexed carbon nanotubes by electron diffraction: Application to double-walled nanotubes. *J Phys D* 42(12):125412.
29. Nanot S, et al. (2013) Broadband, polarization-sensitive photodetector based on optically-thick films of macroscopically long, dense, and aligned carbon nanotubes. *Sci Rep* 3:1335.
30. Miyauchi Y, Oba M, Maruyama S (2006) Cross-polarized optical absorption of single-walled nanotubes by polarized photoluminescence excitation spectroscopy. *Phys Rev B* 74(20):205440.
31. Uryu S, Ando T (2006) Exciton absorption of perpendicularly polarized light in carbon nanotubes. *Phys Rev B* 74(15):155411.
32. Choi S, Deslippe J, Capaz RB, Louie SG (2013) An explicit formula for optical oscillator strength of excitons in semiconducting single-walled carbon nanotubes: family behavior. *Nano Lett* 13(1):54–58.
33. González J, Guinea F, Vozmediano MAH (1996) Unconventional quasiparticle lifetime in graphite. *Phys Rev Lett* 77(17):3589–3592.
34. Hertel T, et al. (2008) Intersubband decay of 1-D exciton resonances in carbon nanotubes. *Nano Lett* 8(1):87–91.
35. Huang SM, Cai XY, Liu J (2003) Growth of millimeter-long and horizontally aligned single-walled carbon nanotubes on flat substrates. *J Am Chem Soc* 125(19): 5636–5637.

Supporting Information

Liu et al. 10.1073/pnas.1318851111

SI Text

Determine the Chiral Index and Absorption Spectrum of the Same Individual Carbon Nanotube. The Si/SiO_2 substrate is etched with open slit, on top of which suspended nanotubes are directly grown. Transmission electron microscope (TEM) beam and laser beam can both go through the slit. This design enables the combination of TEM electron diffraction and optical absorption spectroscopy techniques to investigate the chiral index and absorption cross-section of the same individual suspended carbon nanotubes.

Determine the Nanotube Absorption Constants $\alpha_{//}$ and $\alpha_{\perp}$ from the Homodyne Modulation Signal. In our experiment, we fix the relative angle between the first polarizer (P_1) to the nanotube axis as $\pi/4$. The second polarizer (P_2) is placed close to $\pi/2$ relative to the first polarizer with small deviation angle δ. The intensity modulation is characterized by absorption constants $\alpha_{//}$ and $\alpha_{\perp}$ for light polarized parallel and perpendicular to the nanotube axis, respectively. As described in the main text, $\alpha_{//}$ and $\alpha_{\perp}$ are

$$\begin{aligned}\alpha_{//} &= -\frac{2|E^{//}_{NT}|}{|E^{//}_{in}|}\cos\phi_{//} = \frac{-2|E^{//}_{NT}|}{|E_{in}|\cos\left(\frac{\pi}{4}\right)}\cos\phi_{//},\\ \alpha_{\perp} &= -\frac{2|E^{\perp}_{NT}|}{|E^{\perp}_{in}|}\cos\phi_{\perp} = \frac{-2|E^{\perp}_{NT}|}{|E_{in}|\cos\left(\frac{\pi}{4}\right)}\cos\phi_{\perp}.\end{aligned} \quad [S1]$$

Here, E_{in} is the incident electric field after the first polarizer; $E^{//}_{NT}(E^{\perp}_{NT})$ and $E^{//}_{in}(E^{\perp}_{in})$ are nanotube scattered field and the incident field polarized in the parallel (perpendicular) direction of the nanotube axis, respectively; $\phi_{//}$ ($\phi_{\perp}$) is the relative phase between $E^{//}_{NT}(E^{\perp}_{NT})$ and $E^{//}_{in}(E^{\perp}_{in})$; the $\cos(\pi/4)$ term comes from $\pi/4$ angle between the first polarizer and nanotube axis.

As for homodyne detection, $E^{//}_{NT}$ and $E^{\perp}_{NT}$ will combine at the second polarizer with their respective projection ratio $\cos(\pi/4-\delta)$ and $\cos(3\pi/4-\delta)$; meanwhile, incident electric field E_{in} will be converted to $E_{LO} = E_{in}\sin(\delta)$ by the second polarizer. Therefore, the homodyne modulation signal ($\Delta I/I$) is

$$\begin{aligned}-\frac{\Delta I}{I}(\delta) &= \frac{-2\left[|E^{//}_{NT}|\cos\left(\frac{\pi}{4}-\delta\right)\cos\phi_{//} + |E^{\perp}_{NT}|\cos\left(\frac{3\pi}{4}-\delta\right)\cos\phi_{\perp}\right]}{|E_{in}|\sin(\delta)}\\ &= \frac{1}{\sin(\delta)}\left[\alpha_{//}\cos\left(\frac{\pi}{4}\right)\cos\left(\frac{\pi}{4}-\delta\right) + \alpha_{\perp}\cos\left(\frac{\pi}{4}\right)\cos\left(\frac{3\pi}{4}-\delta\right)\right]\\ &= \frac{\alpha_{//}-\alpha_{\perp}}{2}\mathrm{ctg}(\delta) + \frac{\alpha_{//}+\alpha_{\perp}}{2}.\end{aligned} \quad [S2]$$

In principle, $\alpha_{//}$ and $\alpha_{\perp}$ can be extracted from any two intensity modulation signals taken at two different δ angles. For example, if we use $\pm\delta$ to yield two modulation signals $\Delta I/I(\pm\delta)$, the absorption constants can be expressed as

$$\begin{aligned}\alpha_{//} &= \frac{\Delta I/I(-\delta)-\Delta I/I(\delta)}{2}\tan(\delta) - \frac{\Delta I/I(\delta)+\Delta I/I(-\delta)}{2},\\ \alpha_{\perp} &= \frac{\Delta I/I(\delta)-\Delta I/I(-\delta)}{2}\tan(\delta) - \frac{\Delta I/I(\delta)+\Delta I/I(-\delta)}{2}.\end{aligned} \quad [S3]$$

In our experiment, we used several pairs of $\Delta I/I(\pm\delta)$ and obtained the absorption constants $\alpha_{//}$ and $\alpha_{\perp}$ through fitting. One example of $\alpha_{//}$ and $\alpha_{\perp}$ for (24,24) SWNT is shown in Fig. S3.

Determine the Absolute Absorption Cross-Section from Absorption Constants. The spatial profile of the supercontinuum at the focus has a Gaussian form and can be described as

$$E = E_0\cdot\exp\left(-\frac{(x-x_c)^2+(y-y_c)^2}{R^2}\right), \quad [S4]$$

where x_c and y_c are the coordinates of the center position of the focus and R is a measure of the beam size. For a 1D nanotube along y direction and positioned at x, the absorption signal integrated over the nanotube length is

$$\alpha = \sigma\frac{\sqrt{2\pi}}{S_0}\cdot\frac{d}{R}\cdot\exp\left(-\frac{2(x-x_c)^2}{R^2}\right), \quad [S5]$$

where σ is the absorption cross-section per atom, S_0 is the area per carbon atom in graphitic lattice, and d is the nanotube diameter. We systematically measured the absorption spectra with the nanotube at different positions in the focused beam. Fig. S6 shows the absorption signal at 710 and 640 nm, from which we can determine the beam radius R and center position x_c by fitting. We performed the fitting for all wavelengths in our spectral range. With the beam size information, we obtain absolute values of the nanotube absorption cross-section in the whole spectral range.

Cutting Line Scheme of Optical Transitions with Angular Momentum Difference of $\pm\hbar$ in Carbon Nanotubes. Based on angular momentum selection rule, optical transitions between subbands with angular momentum difference of $\pm\hbar$ are allowed, and indeed S_{12} and S_{21} transitions have been observed by many research groups. However, detailed theoretical analysis (1) shows that S_{12} and S_{21} transitions are really exceptions. Optical resonances for all other higher-order perpendicular transitions are suppressed because the optical transition matrix element is zero at the band gap.

Interestingly, the suppression of higher-order perpendicular transitions can be understood as a direct consequence of the pseudospin of Dirac electrons in graphene. As illustrated in Fig. S4, transitions between subbands with angular momentum difference of $\pm\hbar$ correspond to transitions between adjacent parallel lines in the graphene Brillouin zone in the zone-folding picture, and the electrical field direction is parallel to the momentum of band gap electrons (red dots in Fig. S4) in the graphene Brillouin zone. When the electrical field and electron momentum are parallel to each other, the pseudospin of Dirac electron has to be conserved. For parallel lines at the same side of the K point, conduction and valence states have opposite pseudospin. Therefore, higher-order transitions associated with parallel lines at the same side of K point (Fig. S4), such as E_{13} and E_{24}, are forbidden. E_{12} and E_{21} transitions, however, are special because the two parallel lines are on the opposite side of the K point. In this case, valence electron in the first subband and conduction electron in the second subband have the same pseudospin, and the transitions are allowed.

Empirical Formula for Absorption Cross-Section of an (n,m) Nanotube. We developed an empirical description of the absorption cross-section of an (n,m) nanotube based on the experimentally

extracted parameters. Each transition will contribute a Lorentzian peak and a tail at the higher-energy side described by

$$\frac{\Sigma_p}{\pi}\cdot\frac{w_p}{(E-E_p)^2+w_p^2}+\frac{\Sigma_p}{a\cdot\pi}\cdot\mathrm{conv}\left(\frac{b\cdot w_p}{E^2+(b\cdot w_p)^2},\frac{\Theta[E-(E_p+\Delta)]}{\sqrt{E-(E_{ii}+\Delta)}}\right), \quad \textbf{[S6]}$$

where Θ is the heavyside step function, conv is the convolution operation, E_p, Σ_p, and w_p are, respectively, the excitonic peak energy, oscillator strength, and half-linewidth for each optical transition; a, b, and Δ describe, respectively, the oscillator strength, energy broadening, and energy offset of the higher-energy tail relative to the exciton transition, and they are set as constants for all transitions in a given carbon nanotube. The p is an integer indexing optical transitions of both semiconducting (S_{ii}) and metallic nanotubes (M_{ii}) starting from 1 in the order of S_{11}, S_{22}, M_{11}, S_{33}, S_{44}, M_{22}, S_{55}, S_{66}, M_{33}, S_{77},.... Sum of contributions (value of Eq. **S6**) from all resonances at a particular energy gives the total absorption cross-section at that energy. Resonance peak positions are known from the nanotube optical transition atlas established by Raleigh scattering spectroscopy in our recent work (2). The oscillator strength and linewidth follow empirical scaling laws described in the text. Parameters a, b, and Δ are also approximated empirically as linear functions of nanotube diameter. All of the parameters are summarized in Table S1. This phenomenological description reproduces the absorption spectra within 20% accuracy in our experimental energy region 1.45–2.55 eV. One representative comparison with the experimental data is shown in Fig. S5.

1. Uryu S, Ando T (2006) Exciton absorption of perpendicularly polarized light in carbon nanotubes. *Phys Rev B* 74:155411.

2. Liu K, et al. (2012) An atlas of carbon nanotube optical transitions. *Nat Nanotechnol* 7(5):325–329.

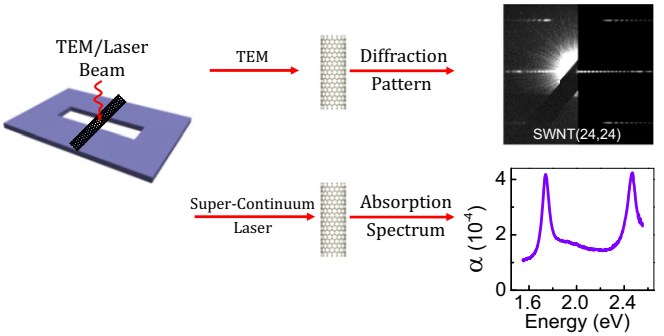

Fig. S1. Scheme of combined single-nanotube TEM electron diffraction and absorption techniques.

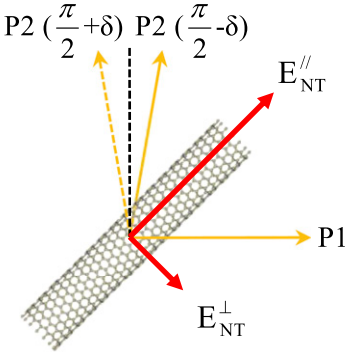

Fig. S2. Geometric setting of two polarizers and the nanotube.

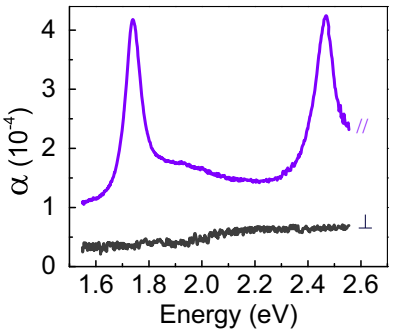

Fig. S3. Absorption of (24,24) single-walled carbon nanotubes with parallel and perpendicular polarization.

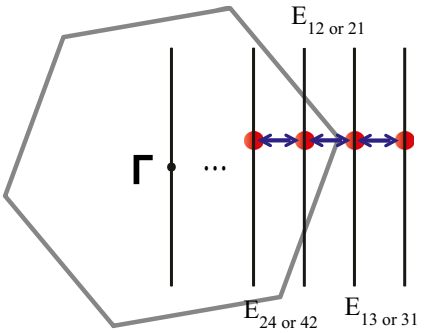

Fig. S4. Cutting line scheme of optical transitions between subbands with angular momentum difference of $\pm\hbar$ in nanotubes.

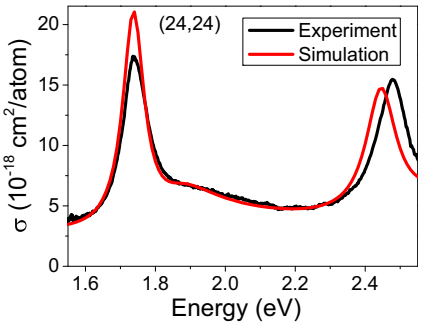

Fig. S5. Experimental data (black) and empirical prediction of absorption cross-section (red) of (24,24) nanotube.

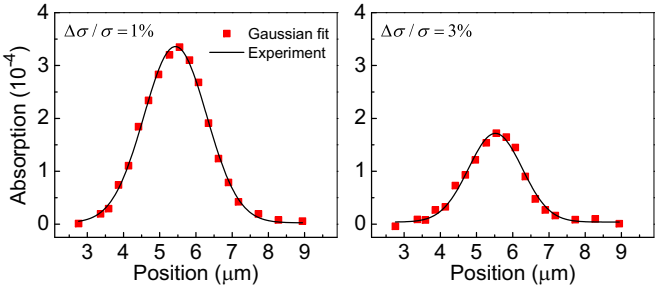

Fig. S6. Dependence of absorption at 710 nm (*Left*) and 640 nm (*Right*) on nanotube position in the beam focus and its fitting to Gaussian function of Eq. **S5**.

Table S1. Parameters for the empirical description of absorption cross-section

	Semiconducting	Metallic
Σ_p	$45.9/[(p + 7.5)d]$	$45.9/[(p + 7.5)d]$
w_p	$0.0194 \cdot E_p$	$0.0214 \cdot E_p$
a	$4.673 - 0.747 \cdot d$	$0.976 + 0.186 \cdot d$
b	$0.97 + 0.256 \cdot d$	$3.065 - 0.257 \cdot d$
Δ	$0.273 - 0.041 \cdot d$	$0.175 - 0.0147 \cdot d$

Σ_p is in unit of 10^{-18} eV·cm^2 per atom; w_p and Δ are in unit of eV; a and b are dimensionless numbers; d is in unit of nm; p is an integer indexing optical transitions of both semiconducting (S_{ii}) and metallic nanotubes (M_{ii}) starting from 1 in the order of S_{11}, S_{22}, M_{11}, S_{33}, S_{44}, M_{22}, S_{55}, S_{66}, M_{33}, S_{77},....